

Mechanical and thermodynamic properties of the monoclinic and orthorhombic phases of SiC_2N_4 under high pressure from first principles

This content has been downloaded from IOPscience. Please scroll down to see the full text.

2014 Chinese Phys. B 23 127101

(<http://iopscience.iop.org/1674-1056/23/12/127101>)

View [the table of contents for this issue](#), or go to the [journal homepage](#) for more

Download details:

IP Address: 155.246.15.35

This content was downloaded on 21/02/2015 at 08:57

Please note that [terms and conditions apply](#).

Mechanical and thermodynamic properties of the monoclinic and orthorhombic phases of SiC₂N₄ under high pressure from first principles*

Miao Nan-Xi(苗楠茜)^{a)}, Pu Chun-Ying(濮春英)^{a)}, He Chao-Zheng(何朝政)^{a)}, Zhang Fei-Wu(张飞武)^{b)c)}, Lu Cheng(卢成)^{a)}, Lu Zhi-Wen(卢志文)^{a)}, and Zhou Da-Wei(周大伟)^{a)†},

^{a)} College of Physics and Electronic Engineering, Nanyang Normal University, Nanyang 473061, China

^{b)} Nanochemistry Research Institute, Curtin University, Perth, WA-6845, Australia

^{c)} State Key Laboratory of Ore Deposit Geochemistry, Institute of Geochemistry, Chinese Academy of Sciences, Guiyang 550002, China

(Received 27 April 2014; revised manuscript received 15 June 2014; published online 10 October 2014)

First principles calculations are performed to systematically investigate the electronic structures, elastic and thermodynamic properties of the monoclinic and orthorhombic phases of SiC₂N₄ under pressure. The calculated structural parameters and elastic moduli are in good agreement with the available theoretical values at zero pressure. The elastic constants of the two phases under pressure are calculated by stress-strain method. It is found that both phases satisfy the mechanical stability criteria within 60 GPa. With the increase of pressure, the degree of the anisotropy decreases rapidly in the monoclinic phase, whereas it remains almost constant in the orthorhombic phase. Furthermore, using the hybrid density-functional theory, the monoclinic and orthorhombic phases are found to be wide band-gap semiconductors with band gaps of about 2.85 eV and 3.21 eV, respectively. The elastic moduli, ductile or brittle behaviors, compressional and shear wave velocities as well as Debye temperatures as a function of pressure in both phases are also investigated in detail.

Keywords: SiC₂N₄, density functional theory, Debye temperature, elastic anisotropy

PACS: 71.15.Mb, 62.20.D-, 71.20.-b

DOI: 10.1088/1674-1056/23/12/127101

1. Introduction

Superhard materials are widely used in the industry for making various tools and coatings, due to their superior mechanical properties.^[1-5] Since the “hard” C₃N₄ was predicted theoretically in the 1980s, extensive theoretical and experimental efforts have been devoted to finding new superhard materials.^[6-14] In recent years, a new class of ternary silicon carbon nitride (Si-C-N) materials have attracted intense attention.^[15-24] Those compounds were originally proposed theoretically for potential superhard materials,^[18-21] then two crystalline solids in the ternary Si-C-N systems, Si₂CN₄ and SiC₂N₄, were synthesized successfully at ambient pressure and high temperature.^[22] Unfortunately, Wang *et al.*^[23] calculated the Vickers hardness of the two phases and found that they are not superhard materials. However, they predicted several stable phases of SiC₂N₄ and Si₂CN₄ compounds under pressure. Moreover, the *Cmmm* structured SiC₂N₄ and *C2/m* and *P2₁/m* structured Si₂CN₄ were believed to be potential superhard materials with a calculated Vickers hardness value exceeding 50 GPa. Recently, Ding *et al.*^[24] also designed the ternary nitrides (Si₂CN₄ and SiC₂N₄) by the substitution method and investigated the mechanical and thermodynamic properties of the ternary nitrides.

Up to now, five structures of SiC₂N₄ have been reported, the ambient-pressure structure (space group *Pn3m*) found in experiment,^[22] the two structures (space groups *C2/m* and *Cmmm*) proposed by Wang *et al.*^[23] and other two structures (space groups *Fd-3m* and *P4-2m*) designed by Ding *et al.*^[24] Although the enthalpy curves, hardness values, phonon curves, and electronic structures of *C2/m* and *Cmmm* SiC₂N₄ have been reported,^[23] for superhard materials, it is also necessary to examine the pressure influences on their elastic stiffness and thermodynamic properties. The primary purpose of this work is to investigate the pressure influences on the properties of the two phases from a thermodynamics point of view. The structural, electronic properties, elastic and mechanical properties of the two phases under pressure are investigated in detail.

2. Computational methods

The calculations in this work were performed using CASTEP code,^[25] which is based on density functional theory (DFT).^[26,27] The exchange-correlation functional was described within the generalized gradient approximation (GGA) as parameterized by Perdew, Burke, and Ernzerhof (PBE).^[28] The interactions between electrons and core ions were treated

*Projected supported by the Henan Joint Funds of the National Natural Science Foundation of China (Grant Nos. U1304612, U1404608, and U1404216), the Special Fund for the Theoretical Physics of China (Grant No. 11247222), the Nanyang Normal University Science Foundation, China (Grant Nos. ZX2010011, ZX2012018, and ZX2014088), the National Natural Science Foundation of China (Grant Nos. 11304167 and 51374132), the Postdoctoral Science Foundation of China (Grant No. 20110491317), and the Young Core Instructor Foundation of Henan Province, China (Grant No. 2012GGJS-152).

†Corresponding author. E-mail: zhoudawei@nynu.edu.cn

with ultrasoft pseudopotentials.^[29] The Si: $3s^23p^2$, C: $2s^22p^2$, and N: $2s^22p^3$ orbitals were explicitly included as valence electrons. The k point separation in Brillouin zone of the reciprocal space was 0.03 \AA . The tolerances for the geometry optimization were as follows: the total energy difference convergent within $5 \times 10^{-6} \text{ eV/atom}$, the maximum Hellmann–Feynman force within 0.01 eV/\AA , the maximum stress within 0.02 GPa , and the maximum atom displacement within $5 \times 10^{-3} \text{ \AA}$. For both phases, a primitive cell of SiC_2N_4 with 7 atoms was used in all the first-principles calculations.

3. Results and discussion

As we have mentioned above, there are five phases of SiC_2N_4 under pressure which have been reported. To investigate the possible phase transition sequence under pressure, we first calculate the relative enthalpies of $Fd-3m$, $P4-2m$, $Pn3m$, and $Cmmm$ phases with respect to $C2/m$ phase as a function of pressure, which are shown in Fig. 1. Both $Fd-3m$ and $P4-2m$ phases designed by Ding *et al.*^[24] using the substitution method have very high enthalpies over the whole pressure range investigated, indicating that they are metastable. The final pressure-induced phase transition sequence of SiC_2N_4 is the cubic structure ($Pn3m$), the monoclinic structure ($C2/m$), and the orthorhombic structure ($Cmmm$). The transition from $Pn3m$ to $C2/m$ phase occurs at around 3.4 GPa , while the transition from $C2/m$ to $Cmmm$ phase takes place at around 25.0 GPa . These values are close to the previous theoretical values of 4 GPa and 29 GPa .^[23]

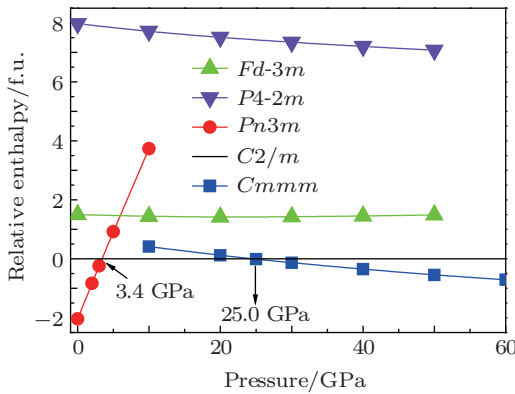


Fig. 1. (color online) Enthalpy differences between $Fd-3m$, $P4-2m$, $Pn3m$, and $Cmmm$ SiC_2N_4 relative to $C2/m$ SiC_2N_4 as a function of pressure.

In Table 1 listed are the calculated equilibrium lattice parameters, bulk modulus B , shear modulus G , Young's modulus E , and Poisson's ratio ν of $C2/m$ and $Cmmm$ phases at zero pressure together with the previous results.^[23] These calculated values agree reasonably with the previous theoretical results,^[23] indicating the rationality of our selected pseudopotential and exchange–correlation function. Furthermore, the equilibrium lattice constant ratios a/a_0 , b/b_0 , and c/c_0 (where

a_0 , b_0 , c_0 are the equilibrium lattice constants at zero pressure and temperature respectively) of the two phases as a function of pressure are plotted in Fig. 2. It is found that the axial compression of both phases can be accurately described by fitting the calculated data, and we can obtain the following relationships at $T = 0 \text{ K}$: ($R^2 > 0.9999$, where R is the correlation coefficient), for crystal structure of $C2/m$ SiC_2N_4 :

$$a/a_0 = 0.99948 - 2.21 \times 10^{-3} \times P + 2.01187 \times 10^{-5} P^2 - 0.992458 \times 10^{-7} \times P^3, \quad (1)$$

$$b/b_0 = 1.00005 - 0.844649 \times 10^{-3} \times P + 0.235638 \times 10^{-5} \times P^2 - 0.747421 \times 10^{-9} \times P^3, \quad (2)$$

$$c/c_0 = 0.99949 - 1.63 \times 10^{-3} \times P + 1.90172 \times 10^{-5} \times P^2 - 1.04119 \times 10^{-7} \times P^3, \quad (3)$$

while for crystal structure of $Cmmm$ SiC_2N_4 ,

$$a/a_0 = 0.99997 - 1.01 \times 10^{-3} \times P + 0.489096 \times 10^{-5} \times P^2 - 0.166999 \times 10^{-7} \times P^3, \quad (4)$$

$$b/b_0 = 1.00021 - 0.924733 \times 10^{-3} \times P + 0.762224 \times 10^{-5} \times P^2 - 0.453523 \times 10^{-7} \times P^3, \quad (5)$$

$$c/c_0 = 0.99998 - 0.816787 \times 10^{-3} \times P + 0.375936 \times 10^{-5} \times P^2 - 0.125597 \times 10^{-7} \times P^3. \quad (6)$$

We note that when the pressure increases, the compression along the a axis is much larger than along the c or b axis in the basal plane for both phases. For $C2/m$ phase, the b axis has lower compressibility than the c axis. However, for $Cmmm$ phase, the compression along the b axis is nearly the same as along the c axis in the basal plane.

Table 1. Calculated equilibrium lattice parameters a , b , and c (\AA), bulk modulus B (GPa), shear modulus G (GPa), Young's modulus E (GPa), and Poisson's ratios ν for $C2/m$ and $Cmmm$ SiC_2N_4 compared with previous theoretical results at zero pressure.

	$C2/m$		$Cmmm$	
	This work	Other work ^[23]	This work	Other work ^[23]
a	9.233	9.257	4.983	4.974
b	2.615	2.607	7.386	7.372
c	4.365	4.364	2.490	2.488
B	193.0	–	325.0	325.7
G	220.1	–	369.5	367.7
E	448.0	–	753.9	754.3
ν	0.16	–	0.16	0.16

In fact, the superhard materials are often found to be wide band gap semiconductors. The band gap energy of $Cmmm$ SiC_2N_4 in previous work^[23] was calculated to be 1.8 eV by means of the density functional theory (DFT). As is well known, DFT always underestimates band gap energy, thus in this paper, we recalculate the band structures and the total densities of states (DOSs) of the two phases using the more accurate hybrid density functional theory (HSE).^[30] The band structures and DOSs of $C2/m$ phase at 4 GPa and $Cmmm$ phase

at 25 GPa are shown in Figs. 3(a) and 3(b), respectively. The Fermi energy level E_f is chosen to be located at the position of 0 eV. For $C2/m$ phase, the top of the valence-band maximum (VBM) and the bottom of conduction-band minimum (CBM) occur at different points, which indicates that it is an indirect semiconductor. The band gap of $C2/m$ phase is calculated to be around 2.85 eV. It is also found that $Cm\bar{m}\bar{m}$ SiC_2N_4 is a wide band gap semiconductor with an energy gap of about 3.21 eV. Furthermore, both VBM and CBM occur at T point, therefore $Cm\bar{m}\bar{m}$ phase is a direct band gap semiconductor.

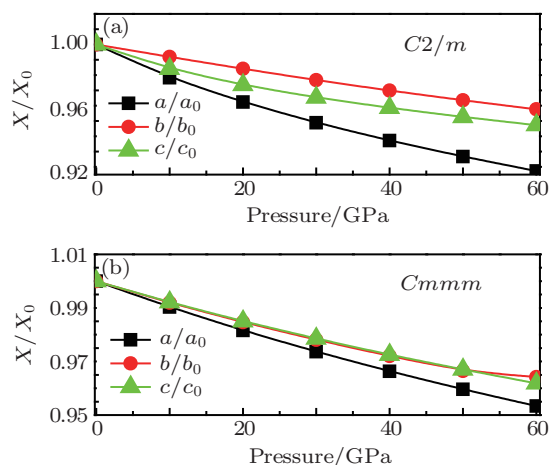


Fig. 2. (color online) Structural parameter ratios a/a_0 , b/b_0 , c/c_0 as a function of pressure for (a) $C2/m$ SiC_2N_4 and (b) $Cm\bar{m}\bar{m}$ SiC_2N_4 , where a_0 , b_0 , and c_0 represent the lattice parameters determined at zero pressure, respectively.

In previous work,^[23] according to the analysis of partial density of states, the Si–N and C–N bonding are found to be mainly governed by the strong hybridization of Si-p and C-p with N-p states. Compared with the partial density of states, Mulliken population analysis^[31] can provide a means of estimating partial atomic charge transformation qualitatively. To

investigate the bonding behaviors of the two phases under pressure, Mulliken charge populations are presented in Table 2. The valence electron configurations are C: $2s^22p^2$, N: $2s^22p^3$, Si: $3s^23p^2$. For both phases, a charge transfer from C atoms and Si atoms to N atoms was observed. Specifically, C-s, Si-s, and Si-p orbitals lose charges and transfer them to N-p orbital. In addition, more charges transfer from Si atoms to N atoms for both phases with the increase of pressure, thus the interactions between N and Si atoms are enhanced by applied pressure.

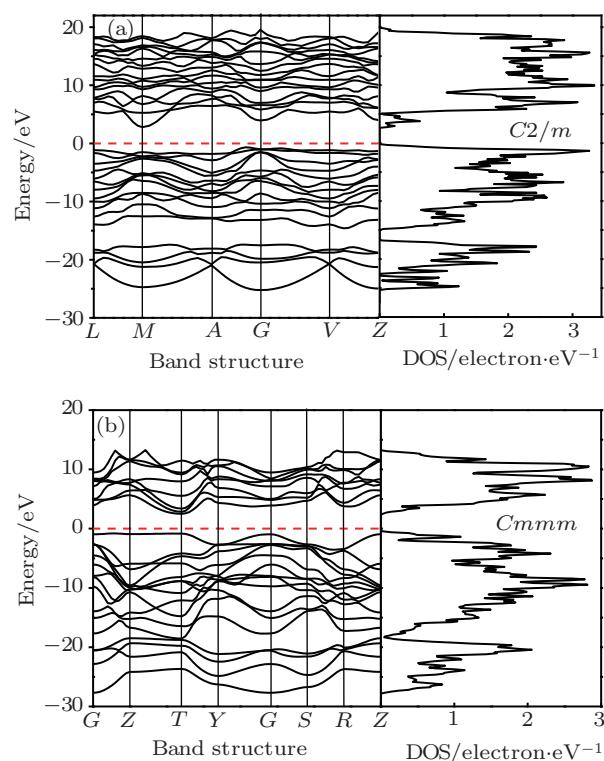


Fig. 3. (color online) Band structures and total densities of states for (a) $C2/m$ SiC_2N_4 at 4 GPa and (b) $Cm\bar{m}\bar{m}$ SiC_2N_4 at 25 GPa.

Table 2. Mulliken charge populations for $C2/m$ and $Cm\bar{m}\bar{m}$ SiC_2N_4 at different pressures.

Structures	Pressure/GPa	Species	Ion	s (e)	p (e)	Total (e)	charge (e)
$C2/m$	0	C	1	1.04	2.52	3.56	0.44
		N	1	1.52	4.43	5.95	-0.95
		N	2	1.60	3.81	5.41	-0.41
		Si	1	0.73	1.42	2.15	1.85
	40	C	1	1.00	2.55	3.56	0.44
		N	1	1.51	4.45	5.96	-0.96
		N	2	1.56	3.88	5.44	-0.44
		Si	1	0.67	1.42	2.09	1.91
$Cm\bar{m}\bar{m}$	0	C	1	1.05	2.52	3.57	0.43
		N	1	1.46	4.14	5.61	-0.61
		N	2	1.56	4.12	5.67	-0.67
		Si	1	0.76	1.54	2.30	1.70
	40	C	1	1.01	2.56	3.57	0.43
		N	1	1.44	4.19	5.62	-0.62
		N	2	1.53	4.17	5.70	-0.70
		Si	1	0.70	1.52	2.22	1.78

The elastic properties of a solid are important. They are not only closely related to various fundamental solid-state phenomena, such as interatomic bonding, equations of state, and phonon spectra, but also connected thermodynamically with specific heat, thermal expansion, Debye temperature, and Grüneisen parameter. In order to study the mechanical stability of SiC_2N_4 , we calculated the second-order elastic constants C_{ij} using the “stress–strain method”. The calculated elastic constants as a function of pressure are shown in Fig. 4. For $C2/m$ SiC_2N_4 , there are thirteen independent elastic constants, while for $Cmmm$ SiC_2N_4 , there are only nine independent elastic constants. As is well known, the elastic constants C_{11} , C_{22} ,

C_{33} character the resistances to linear compression in x , y , and z directions, respectively, while the elastic constants C_{12} , C_{13} , and C_{23} and C_{44} , C_{55} , and C_{66} are related to the elasticity in shape. For $C2/m$ SiC_2N_4 , C_{35} and C_{46} decrease gradually with the increase of pressure, while C_{12} , C_{13} , C_{23} , C_{25} , C_{44} , C_{55} , C_{66} , and C_{15} all increase linearly with pressure increasing. In addition, as pressure increases, the elastic constants C_{11} and C_{33} have a crossover point at around 11 GPa. For $Cmmm$ SiC_2N_4 , C_{33} is highest in all the elastic constants and C_{22} and C_{11} follow it, implying that they are incompressible under uniaxial stress along the coordinate axis. Besides, C_{12} , C_{13} , C_{23} , C_{44} , C_{55} , and C_{66} increase slowly with pressure increasing.

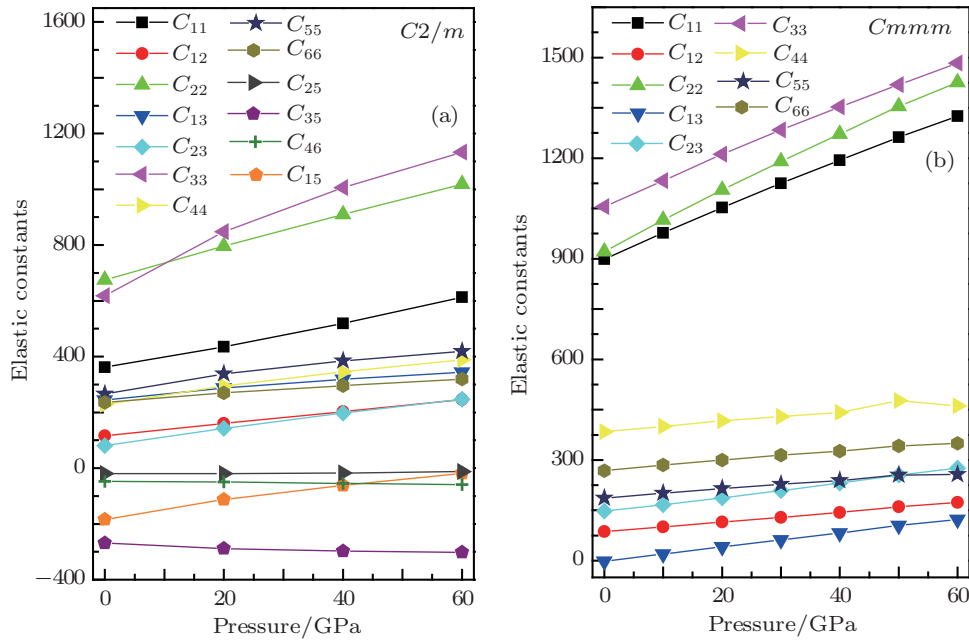


Fig. 4. (color online) Calculated pressure dependences of elastic constants for (a) $C2/m$ SiC_2N_4 and (b) $Cmmm$ SiC_2N_4 .

As for the mechanical stability of a structure, one condition is that its strain energy must be positive against any homogeneous elastic deformation. For monoclinic structure, the mechanical stability criterion can be expressed as^[32]

$$\begin{aligned}
 &C_{11} > 0, \quad C_{22} > 0, \quad C_{33} > 0, \quad C_{44} > 0, \quad C_{55} > 0, \quad C_{66} > 0, \\
 &[C_{11} + C_{22} + C_{33} + 2(C_{12} + C_{13} + C_{23})] > 0, \\
 &(C_{33}C_{55} - C_{35}^2) > 0, \quad (C_{44}C_{66} - C_{46}^2) > 0, \\
 &(C_{22} + C_{33} - 2C_{23}) > 0, \\
 &[C_{22}(C_{33}C_{55} - C_{35}^2) + 2C_{23}C_{25}C_{35} - C_{23}^2C_{55} - C_{25}^2C_{33}] > 0, \\
 &\{2[C_{15}C_{25}(C_{33}C_{12} - C_{13}C_{23}) + C_{15}C_{35}(C_{22}C_{13} - C_{12}C_{23}) \\
 &\quad + C_{25}C_{35}(C_{11}C_{23} - C_{12}C_{13})] - [C_{15}^2(C_{22}C_{33} - C_{23}^2) \\
 &\quad + C_{25}^2(C_{11}C_{33} - C_{13}^2) + C_{35}^2(C_{11}C_{22} - C_{12}^2) + C_{55}g]\} > 0, \\
 &g = C_{11}C_{22}C_{33} - C_{11}C_{23}^2 - C_{22}C_{13}^2 - C_{33}C_{12}^2 + 2C_{12}C_{13}C_{23}. \quad (7)
 \end{aligned}$$

For orthorhombic structure, the mechanical stability criterion

can be expressed as^[32]

$$\begin{aligned}
 &C_{11} > 0, \quad C_{22} > 0, \quad C_{33} > 0, \quad C_{44} > 0, \quad C_{55} > 0, \quad C_{66} > 0, \\
 &C_{11} + C_{22} + C_{33} + 2(C_{12} + C_{13} + C_{23}) > 0, \\
 &C_{11} + C_{22} - 2C_{12} > 0, \quad C_{11} + C_{33} - 2C_{13} > 0, \\
 &C_{22} + C_{33} - 2C_{23} > 0. \quad (8)
 \end{aligned}$$

The calculated results for the two structures all satisfy the above stability criteria over the whole pressure range investigated, implying that the two structures are mechanically stable within 60 GPa.

Based on the calculated elastic constants, we deduce the bulk modulus B , shear modulus G , Young’s modulus E , Poisson ratio ν , and B/G which are widely used to describe the mechanical behaviors of materials. As suggested by Voigt,^[33] the polycrystalline bulk modulus B_V and shear modulus G_V can be expressed in the appropriate combinations of single-

crystal elastic constants C_{ij} ,

$$9BV = (C_{11} + C_{22} + C_{33}) + 2(C_{12} + C_{23} + C_{13}), \quad (9)$$

$$15G_V = (C_{11} + C_{22} + C_{33}) - (C_{12} + C_{23} + C_{13}) + 3(C_{44} + C_{55} + C_{66}), \quad (10)$$

Analogously, Reuss and Angew^[34] have derived the bulk modulus B_R and shear modulus G_R expressions in terms of compliance constants S_{ij} as follows:

$$\frac{1}{B_R} = (S_{11} + S_{12} + S_{33}) + 2(S_{12} + S_{23} + S_{13}), \quad (11)$$

$$\frac{15}{G_R} = 4(S_{11} + S_{22} + S_{33}) - 4(S_{12} + S_{23} + S_{13}) + 3(S_{44} + S_{55} + S_{66}). \quad (12)$$

Let S_{ij} be the elastic compliance constants:

$$\begin{aligned} S_{11} &= (C_{22}C_{33} - C_{23}^2)/\Delta, & S_{22} &= (C_{11}C_{33} - C_{13}^2)/\Delta, \\ S_{33} &= (C_{11}C_{22} - C_{12}^2)/\Delta, & S_{12} &= (C_{13}C_{23} - C_{12}C_{23})/\Delta, \\ S_{13} &= (C_{12}C_{23} - C_{13}C_{22})/\Delta, & S_{23} &= (C_{12}C_{13} - C_{11}C_{23})/\Delta, \\ S_{ii} &= 1/C_{ii}, \quad (i = 4, 5, 6), \end{aligned}$$

with

$$\begin{aligned} \Delta &= C_{13}(C_{12}C_{23} - C_{13}C_{22}) + C_{23}(C_{12}C_{13} - C_{23}C_{11}) \\ &\quad + C_{33}(C_{11}C_{22} - C_{12}^2). \end{aligned} \quad (13)$$

Hill^[35] has shown that for any crystalline structure, the assumptions of Voigt and Reuss lead to an upper bound and a lower bound of B and G , respectively. In solid state physics, it is common to use the arithmetic average of Voigt and Reuss bounds for the evaluation of B and G , which is called the Voigt–Reuss–Hill (VRH) approximation.

$$B = \frac{B_V + B_R}{2}, \quad G = \frac{G_V + G_R}{2}. \quad (14)$$

The polycrystalline Young's modulus (E) and the Poisson's ratio (ν) are then calculated using the relationships^[35]

$$E = \frac{9BG}{3B + G}, \quad \nu = \frac{3B - 2G}{6B + 2G}. \quad (15)$$

The bulk modulus reflects the resistance of a material to a volume change and its response to a hydrostatic pressure, whereas the shear modulus describes the resistance of a material to a shape change. The aggregate bulk, shear, and Young's moduli of both phases as a function of pressure are shown in Figs. 5(a) and 5(b), respectively. Both the bulk and shear moduli increase with the increase of pressure. The calculated bulk moduli of both phases under pressure are larger than 200 GPa, which are comparable to those of classic hard materials, such as β -B₂O₃ (169.9 GPa)^[36] and α -Al₂O₃ (253.7 GPa).^[37] It can also be seen that the three curves show similar trends under elevated pressure but they vary at different rates, particularly under higher pressure. The *Cmmm* phase has larger

bulk, shear, and Young's modulus than *C2/m* phase in the whole pressure range studied, indicating that *Cmmm* SiC₂N₄ is harder than *C2/m* SiC₂N₄.

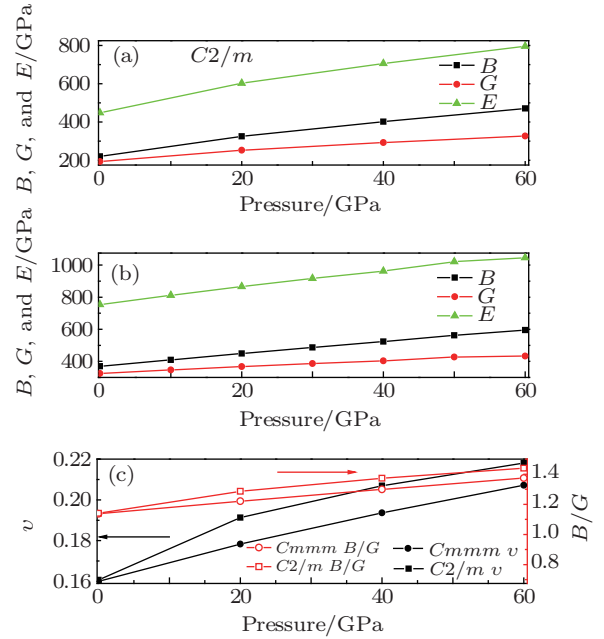


Fig. 5. (color online) Bulk, shear, and Young's moduli of (a) *C2/m* SiC₂N₄ and (b) *Cmmm* SiC₂N₄ as a function of pressure; (c) The Poisson's ratios ν and B/G for *C2/m* and *Cmmm* SiC₂N₄.

For the application of materials, the brittle or ductile behavior is of great importance. Pugh^[38] proposed a formula, i.e., B/G , to judge a metal's ductility and brittleness in 1954. The critical value which distinguishes between ductile material and brittle material has been evaluated to be 1.75. If $B/G > 1.75$, material behaves in a ductile manner, if not, a material demonstrates brittleness. Here we calculate the values of B/G for SiC₂N₄ to investigate the brittleness of the two phases under pressure as shown in Fig. 5(c). It is found that the B/G values of two structures are less than 1.75, thus both phases behave in brittle manners within 60 GPa. With the increase of pressure, B/G values increase for both phases, revealing that the degree of brittleness decreases under applied pressure. In fact, the brittleness and ductility can also be estimated by the Frantsevich rule,^[39] where the critical value of Poisson's ratio is suggested to be 1/3. For brittle materials, $\nu < 1/3$, otherwise the material behaves in a ductile manner. For the two structures, the Poisson ratios are both less than 1/3 as shown in Fig. 5(c), which also suggests that the two SiC₂N₄ compounds exhibit brittle behaviors under pressure.

As is well known, microcracks are easily induced in the materials due to the significant elastic anisotropy.^[40] Hence, it is important to calculate elastic anisotropy in order to improve their mechanical durability. Chuang and Buessem introduced^[41] a concept of percent elastic anisotropy which is a measure of elastic anisotropy possessed by the crystal under consideration. The bulk modulus anisotropic factor A_B and

shear anisotropy A_G are defined as

$$A_B = \frac{B_V - B_R}{B_V + B_R}, \quad A_G = \frac{G_V - G_R}{G_V + G_R}, \quad (16)$$

respectively, where B and G are bulk modulus and shear modulus, and the subscripts V and R represent the Voigt and Reuss bounds. For the two expressions, zero represents complete elastic isotropy and a value of 1 (100%) refers to the largest possible anisotropy. The percentages of bulk and shear anisotropies of $Cmmm$ SiC_2N_4 and $C2/m$ SiC_2N_4 are shown in Fig. 6(a). We observe that on the whole, $Cmmm$ SiC_2N_4 possesses very low bulk and shear anisotropies over the whole pressure range investigated. Furthermore, $Cmmm$ SiC_2N_4 exhibits comparatively small bulk anisotropy, while the value of its shear anisotropy is slightly large. Compared with $Cmmm$ phase, $C2/m$ phase possesses comparatively high anisotropy. Interestingly, as pressure increases, both the anisotropy factors A_B and A_G of $C2/m$ SiC_2N_4 decrease gradually, while the corresponding values of $Cmmm$ SiC_2N_4 remain almost unchanged.

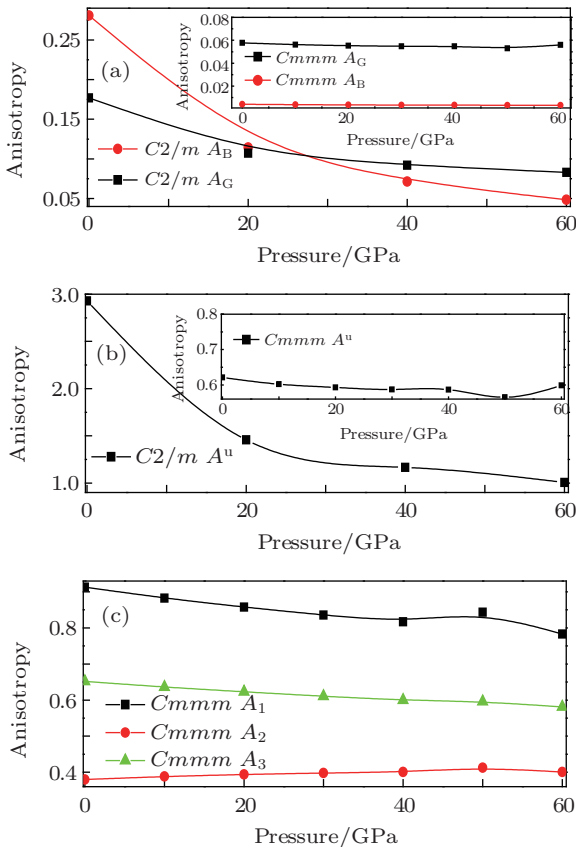


Fig. 6. (color online) Pressure dependences of elastic anisotropies for $Cmmm$ and $C2/m$ SiC_2N_4 ; (a) percentage anisotropy in compressibility A_B and shear A_G ; (b) universal elastic anisotropy A^u ; (c) shear anisotropic factors A_1, A_2 , and A_3 of $Cmmm$ SiC_2N_4 .

In order to study the anisotropy of single crystal quantitatively, another universal elastic anisotropy index A^u was developed by Ranganathan and Ostioja-Starzewski^[42] for crystal

with any symmetry as shown below

$$A^u = 5 \frac{G_V}{G_R} + \frac{B_V}{B_R} - 6. \quad (17)$$

The farther from 0 the value of A^u , the larger the anisotropy of material will be. For isotropy materials, $A^u = 0$. The calculated A^u values of $Cmmm$ and $C2/m$ SiC_2N_4 as a function of pressure are shown in Fig. 6(b). It is found that the universal elastic anisotropy index A^u of $C2/m$ SiC_2N_4 is more sensitive to pressure, while that of $Cmmm$ SiC_2N_4 remains nearly unchanged with increasing the pressure. Those results agree with the above discussion about the percentage of bulk anisotropy and shear anisotropy.

To investigate the degrees of anisotropy of $Cmmm$ SiC_2N_4 in different planes in detail, we further calculate the anisotropy factors of $Cmmm$ SiC_2N_4 as a function of pressure, which are shown in Fig. 6(c). The shear anisotropic factors reflect the degrees of anisotropy in the bonding between atoms in different planes. There are three shear anisotropic factors in the orthorhombic phase,^[40] i.e., A_1 which is the shear anisotropic factor for the $\{100\}$ shear plane between the $\{011\}$ and $\{010\}$ directions, A_2 which is the shear anisotropic factor in the $\{010\}$ shear plane between $\{101\}$ and $\{001\}$ directions, and A_3 which is the shear anisotropic factor in the $\{001\}$ shear plane between $\{110\}$ and $\{010\}$ directions. These factors are expressed as

$$A_1 = 4C_{44}/(C_{11} + C_{33} + 2C_{13}), \quad (18)$$

$$A_2 = 4C_{55}/(C_{22} + C_{33} - 2C_{23}), \quad (19)$$

$$A_3 = 4C_{66}/(C_{11} + C_{22} - 2C_{12}). \quad (20)$$

For an isotropic crystal, all three factors must be one while any other value less or greater than one indicates the degree of anisotropy. When the applied pressure increases from 0 to 60 GPa, the anisotropy factors A_1 and A_3 decrease by approximately 14.2% and 10.8%, respectively, while A_2 increases by approximately 5.5%. However, for $Cmmm$ SiC_2N_4 , the $\{100\}$ shear planes show more isotropic than the $\{010\}$ shear planes as well as the $\{001\}$ shear planes over the whole pressure range investigated.

Debye temperature is another one of fundamental parameters for solid materials, which is correlated with many physical properties, such as thermal expansion, melting point, and Grüneisen parameter.^[40] At low temperatures, Debye temperature Θ_D is proportional to the sound velocity and directly related to the elastic constant through bulk and shear moduli^[43]

$$\Theta_D = \frac{h}{k_B} \sqrt[3]{\frac{3nN_A\rho}{4\pi M}} v_m, \quad (21)$$

where h is the Planck's constant, k_B is the Boltzmann's constant, n is the number of atoms per formula unit, M is the molecular weight, N_A is the Avogadro's number, ρ is the density, and v_m is the average sound velocity. In fact, v_m can be

obtained from the longitudinal wave velocities v_l and transverse wave velocities v_s , i.e., from the following relationship:

$$\frac{3}{v_m^3} = \frac{1}{v_l^3} + \frac{2}{v_s^3}, \quad v_l = [(B + 4/3G)/\rho]^{1/2},$$

$$v_s = (G/\rho)^{1/2}. \quad (22)$$

The calculated velocities and Debye temperatures as a function of pressure for both phases are shown in Fig. 7. For both phases, v_m , v_l , and v_s as well as Θ_D increase monotonically as pressure increases from 0 to 60 GPa. For most materials, usually, the higher the Debye temperature, the larger the microhardness is. The Debye temperature of *Cmmm* SiC₂N₄ is higher than that of *C2/m* SiC₂N₄, implying that the microhardness of *C2/m* SiC₂N₄ is not so good as that of *Cmmm* SiC₂N₄. Furthermore, since Debye temperature in a solid represents the interatomic force, the higher Debye temperature also indicates that *Cmmm* SiC₂N₄ has stronger bonds than *C2/m* SiC₂N₄.

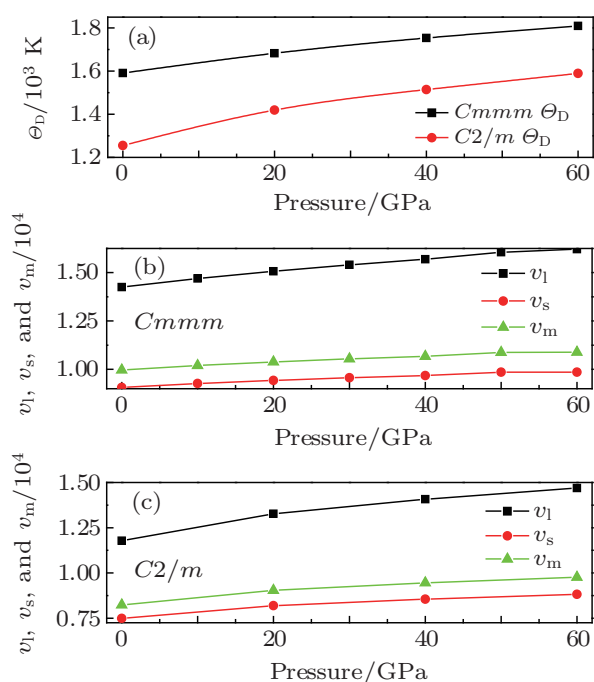


Fig. 7. (color online) (a) Pressure dependences of Debye temperatures of *Cmmm* and *C2/m* SiC₂N₄; pressure dependences of transverse v_s , longitudinal v_l , and average v_m sound velocities of (b) *Cmmm* SiC₂N₄ and (c) *C2/m* SiC₂N₄.

4. Conclusions

In this work, we employ the density functional perturbation theory to investigate the electronic structures, elastic and thermodynamic properties of the two new discovered phases of SiC₂N₄ under pressure. The calculated structural and elastic parameters accord well with previous theoretical values at zero pressure. The *C2/m* phase is an indirect-gap semiconductor, while *Cmmm* phase is a direct-gap semiconductor. The band-gap energies of *C2/m* phase at 4 GPa and *Cmmm* phase

at 25 GPa are calculated to be 2.85 eV and 3.21 eV, respectively. With the increase of pressure, a charge transfer from the C atoms and Si atoms to N atoms is observed for each of both phases. The two phases satisfy the mechanical stable criteria within 60 GPa. With increasing the pressure, the degree of the anisotropy decreases rapidly in monoclinic phase, whereas it remains almost unchanged in orthorhombic phase. For the orthorhombic phase, its $\{1\ 0\ 0\}$ shear planes show more isotropic than the $\{0\ 1\ 0\}$ shear planes as well as the $\{0\ 0\ 1\}$. Furthermore, both phases behave in brittle manners within 60 GPa. However, the degrees of brittleness for the two phases decrease under applied pressure. The shear modulus, bulk modulus, Young's modulus, Poisson's coefficient, and wave velocities as well as Debye temperature are also discussed in this paper, more experimental and theoretical studies are recommended.

References

- [1] Wentorf R H, DeVries R C and Bundy F P 1980 *Science* **208** 873
- [2] Leger J M and Haines J 1997 *Endeavour*. **21** 121
- [3] Brook R J 1999 *Nature* **400** 312
- [4] Brazhkin V V, Lyapin A G and Hemley R J 2002 *Phil. Mag. A* **82** 231
- [5] McMillan P F 2002 *Nat. Mater.* **1** 19
- [6] Teter D M and Hemley R J 1996 *Science* **271** 53
- [7] Kaner R B, Gilman J J and Tolbert S H 2005 *Science* **308** 1268
- [8] Tian Y J, Xu B, Yu D L, Ma Y M, Wang Y B, Jiang Y B, Hu W T, Tang C C, Gao Y F, Luo K, Zhao Z S, Wang L M, Wen B, He J L and Liu Z Y 2013 *Nature* **493** 385
- [9] Zhang X X, Wang Y C, Lv J, Zhu C Y, Li Q, Zhang M, Li Q and Ma Y M 2013 *J. Chem. Phys.* **138** 114101
- [10] Li Q, Liu H Y, Zhou D, Zheng W T, Wu Z J and Ma Y M 2012 *Phys. Chem. Chem. Phys.* **14** 13081
- [11] Xu L F, Zhao Z S, Wang L M, Xu B, He J L, Liu Z Y and Tian Y J 2010 *J. Phys. Chem. C* **114** 22688
- [12] Liu H Y, Li Q, Zhu L and Ma Y M 2011 *Phys. Lett. A* **375** 771
- [13] Li Q, Wang M, Oganov A R, Cui T, Ma Y M and Zou G T 2009 *J. Appl. Phys.* **105** 053514
- [14] Tian F B, Wang J H, He Z, Ma Y M, Wang L C, Cui T, Chen C B, Liu B B and Zou G T 2008 *Phys. Rev. B* **78** 235431
- [15] Gong Z, Wang E G, Xu G C and Chen Y 1999 *Thin Solid Films* **348** 114
- [16] Chen L C, Chen K H, Wei, S L, Kichambare P D, Wu J J, Lu T R and Kuo C T 1999 *Thin Solid Films* **355–356** 112
- [17] Sundaram K B, Alizadeh Z, Todi R M and Desai V H 2004 *Mater. Sci. Eng. A* **368** 103
- [18] Wang C Z, Wang E G and Dai Q Y 1998 *J. Appl. Phys.* **83** 1975
- [19] Lowther J E, Amkreutz M, Frauenheim T, Kroke E and Riedel R 2003 *Phys. Rev. B* **68** 033201
- [20] Zhang X Y, Chen Z W, Du H J, Yang C, Ma M Z, He J L, Tian Y J and Liu R P 2008 *J. Appl. Phys.* **103** 083533
- [21] Du H J, Li D C, He J L, Yu D L, Xu B, Liu Z Y, Wang H T and Tian Y J 2009 *Diamond Relat. Mater.* **18** 72
- [22] Riedel R, Greiner A, Miche G, Dressler W, Fuess H, Bill J and Aldinger F 1997 *Angew. Chem., Int. Ed. Engl.* **36** 603
- [23] Wang H B, Li Q, Wang H, Liu H Y, Cui T and Ma Y M 2010 *J. Phys. Chem. C* **114** 8609
- [24] Ding Y C, Chen M, Jiang M H and Gao X Y 2012 *Physica B* **407** 4323
- [25] Segall M D, Lindan P J D, Probert M J, Pickard C J, Hasnip P J, Clark S J and Payne M C 2002 *J. Phys.: Condens. Matter* **14** 2717
- [26] Hohenberg P and Kohn W 1964 *Phys. Rev. B* **136** 864
- [27] Kohn W and Sham L J 1965 *Phys. Rev. A* **140** 1133
- [28] Perdew J P, Burke K and Ernzerhof M 1996 *Phys. Rev. Lett.* **77** 3865
- [29] Vanderbilt D 1990 *Phys. Rev. B* **41** 7892

- [30] Krukau A V, Vydrov O A, Izmaylov A F and Scuseria G E 2006 *J. Chem. Phys.* **125** 224106
- [31] Mulliken R S 1955 *J. Chem. Phys.* **23** 1833
- [32] Nye J F 1985 *Physical Properties of Crystals* (Oxford: Oxford University Press)
- [33] Voigt W 1928 *Lehrbuch der Kristallphys* (Leipzig: Teubner Press)
- [34] Reuss A and Angew Z 1929 *Math. Mech.* **9** 49
- [35] Hill R 1952 *Proc. Phys. Soc. Lond.* **65** 349
- [36] Nieto Sanz D, Loubeyre P, Crichton W and Mezouar M 2004 *Phys. Rev. B* **70** 214108
- [37] Hu Z G, Yoshimura M, Mori Y and Sasaki T 2004 *J. Cryst. Growth* **260** 287
- [38] Pugh S F 1954 *Philos. Mag.* **45** 823
- [39] Frantsevich I N, Voronov F F and Bokuta S A 1983 *Elastic Constants and Elastic Moduli of Metals and Insulators Handbook* (Kiev: Naukova Dumka)
- [40] Ravindran P, Fast L, Korzhavyi P A, Johnsson B, Wills J and Eriksson O 1998 *J. Appl. Phys.* **84** 4891
- [41] Chung D H and Buessem W R 1968 *Anisotropy in Single-crystal Refractory Compounds: Proceedings* (New York: Plenum Press)
- [42] Ranganathan S I and Ostoja-Starzewski M 2008 *Phys. Rev. Lett.* **101** 055504
- [43] Anderson O L 1963 *J. Phys. Chem. Solids* **24** 909